Rotordynamic Crack Diagnosis: Distinguishing Crack Depth and Location

Philip Varney[1]
e-mail: pvarney3@gatech.edu

Itzhak Green
e-mail: itzhak.green@me.gatech.edu

Woodruff School of Mechanical Engineering,
Georgia Institute of Technology,
Atlanta, GA 30332

The goal of this work is to establish simple condition monitoring principles for diagnosing the depth and location of transverse fatigue cracks in a rotordynamic system. The success of an on-line crack diagnosis regimen hinges on the accuracy of the crack model, which should account for the crack's depth and location. Two gaping crack models are presented; the first emulates a finite-width notch typically manufactured for experimental purposes, while the second models a gaping fatigue crack. The rotordynamic model used herein is based upon an available overhung rotordynamic test rig that was originally constructed to monitor the dynamics of a mechanical face seal. Four degree-of-freedom, linear equations of motion for both crack models are presented and discussed. Free and forced response analyses are presented, emphasizing results applicable to condition monitoring and, particularly, to diagnosing the crack parameters. The results demonstrate that two identifiers are required to diagnose the crack parameters: the 2X resonance shaft speed and the magnitude of the angular 2X subharmonic resonance. First, a contour plot of the 2X resonance shaft speed versus crack depth and location is generated. The magnitude of the 2X resonance along the desired 2X frequency contour is then obtained, narrowing the possible pairs of crack location and depth to either one or two possibilities. Practical aspects of the suggested diagnostic procedure are discussed, as well as qualitative observations concerning crack detection. [DOI: 10.1115/1.4025039]

1 Introduction

Safe and economical operation of rotating machinery necessitates adherence to condition monitoring protocols, the goal of which can be either detection or diagnosis. For the purposes of this work, detection is a binary fault judgment; the condition monitoring system only indicates a fault's presence. Diagnosis improves upon detection by estimating fault parameters. Vibration monitoring has proven particularly adept as a crack detection and diagnosis tool. Rotordynamic vibration monitoring systems typically rely on shaft speed harmonics occurring at integer multiples of the shaft speed [1–4]; the profile of these harmonics often indicates the type and severity of a fault. The goal of this work is to employ the 2X harmonic to detect a gaping transverse fatigue crack and diagnose its location and depth.

The current work on transverse shaft crack diagnosis is an outgrowth of research performed over the past two decades investigating the dynamics of a flexibly mounted rotor (FMR) mechanical face seal system. Green et al. [5,6] developed a kinematic model for two seal types: an FMR and a flexibly mounted stator seal configuration. Lee and Green [7] investigated coupling between the dynamics of the shaft and the seal through the development of the complex extended transfer matrix. An overhung FMR noncontacting mechanical face seal test rig was subsequently constructed to experimentally investigate the face seal dynamics [3] (the rotordynamic model used in this work emulates this overhung test rig). Three eddy-current proximity probes mounted to the stator directly extracted the rotor's angular response. The test rig parameters and data acquisition system are discussed extensively by Lee and Green [8]. During testing, a unique vibratory phenomenon was observed: higher harmonic oscillations in the steady-state rotor response. It was subsequently determined that these higher harmonic oscillations were caused by seal face contact.

Green and Casey [1] and Varney and Green [2] advanced the aforementioned research by studying the feasibility of using the overhung test rig to detect a transverse shaft crack. The test rig's advantage for condition monitoring is that the rotor's angular response is directly extracted using proximity probes, without relying on bearing vibration measurements. A gaping crack is introduced, and the rotor's response is obtained analytically [1,2] and experimentally [2] (the particular models employed will be discussed shortly). The authors concluded that differentiation of seal face contact and shaft cracks is feasible due to differences in the rotor's angular orbit.

It is well known [4,9–11] that cracks can display breathing behavior; the faces of the crack open and close as the shaft rotates. Darpe et al. [10] employed a response-dependent breathing model incorporating a crack closure line to account for a partial open/close state of the crack. Interestingly, the authors discovered that in the neighborhood of subharmonic resonance (the principle regime of interest in this work), the crack remains mostly open. Dimarogonas and Papadopoulos [12] indicated that the assumption of a gaping crack is valid for small static deflections and vibration amplitudes (such as those investigated herein). Additionally, many crack detection concepts were validated experimentally using open cracks (such as notches). Considering the aforementioned conclusions, the analysis of a gaping crack is not necessarily an oversimplification and can provide meaningful condition monitoring results.

In this investigation, a gaping crack is proposed to establish guidelines for crack diagnostics without the additional complexity of crack breathing. Gaping cracks remain open regardless of the shaft's angular orientation, resulting in a stiffness asymmetry that is constant in a shaft-fixed reference frame. Green and Casey [1] employed a gaping fatigue crack (GFC) of negligible width and terminating in a sharp edge. The primary vibration signature of such a crack is the appearance of a 2X harmonic induced by forcing in a constant inertial direction (such as gravity). This observation is corroborated by many other researchers, such as Dimarogonas [12], Mayes [13], and Rao [14] (who provides an intuitive explanation concerning the physical meaning of the 2X harmonic). The presence of a frequency at twice the shaft speed

[1]Corresponding author.

Contributed by the Manufacturing Materials and Metallurgy Committee of ASME for publication in the JOURNAL OF ENGINEERING FOR GAS TURBINES AND POWER. Manuscript received July 5, 2013; final manuscript received July 8, 2013; published online September 17, 2013. Editor: David Wisler.

creates a subharmonic resonance at half of a natural frequency; this 2X resonant shaft speed decreases with increasing crack depth, while the magnitude of the resonant response correspondingly increases. The influence of crack location on detection and diagnostics is not discussed meaningfully in any of these works.

Varney and Green [2] developed a transfer matrix for a finite-width rectangular notch that emulates an experimentally manufactured crack. The steady-state 2X angular response of the overhung rotor was subsequently obtained. It was determined that a GFC is easier to detect than a notch of commensurate depth, as the GFC results in a greater loss of stiffness (corroborated by Silva [15] and Dimarogonas [12]). As expected, the experimental 2X resonance shaft speeds aligned closer to those predicted by the notch model than the gaping fatigue crack model.

Neither of the aforementioned works [1,2] investigate variations in crack location or suggest crack characteristic diagnostic procedures. A significant parameter influencing the rotor response is neglected by only investigating variations in crack depth. Many works similarly neglect or simplify the influence of crack location or propose complicated measurement procedures for distinguishing crack depth and location. Several such procedures are mode shape measurement (or similarly, shaft deflection measurements) [13,16], coupled response measurement [17,18], and active magnetic bearings [19]. Measurement of the shaft deflection profile is difficult in rotordynamic systems [20], as a large number of measurement locations along the rotating shaft are required. Similarly, coupled response measurements and active magnetic bearings require expensive and sophisticated shaft excitation equipment [21]. For these reasons, the present work aims to utilize a well-understood vibration monitoring signal, the 2X harmonic, to diagnose the crack parameters. This work shows that crack depth alone is insufficient in determining fault severity. It will be shown that in conjunction with crack depth, the location of the crack must also be considered. Considering the crack either open or breathing does not affect the premises established in this work, as the concepts are equally applicable to both classifications of cracks.

The compliance matrices are provided for two gaping crack models, the notch and the GFC. Four degree-of-freedom linear equations of motion are developed, including imbalance and gravity excitation. Due to the nature of the overhung test rig and associated monitoring system, the angular degrees of freedom are used for establishing diagnostic principles. A free response analysis provides the 2X resonance shaft speed. Solution of the forced equations of motion gives the rotor's steady-state response, which includes the 2X harmonic. A procedure for diagnosing the crack's location and depth is presented and discussed, along with qualitative observations pertaining to the difficulty of crack detection and diagnosis.

2 Analytic Modeling

Two gaping cracks are investigated: a rectangular notch typically manufactured for experimental purposes and a true fatigue crack of negligible width, the GFC. For both models, the depth and location of the crack comparably influence the rotor's dynamic response; understanding the dynamic interplay between crack location and depth is, thus, crucial for diagnostics.

2.1 Undamaged Rotordynamic System. It is necessary to provide a consistent framework for formulating the dynamics of the undamaged system prior to characterizing the crack's compliance. By using a consistent dynamic framework, the differences between the crack models can be isolated and investigated. A model of an undamaged overhung rotordynamic system is presented, along with relevant degrees of freedom.

The undamaged overhung system is shown in Fig. 1(*a*). The rotor is modeled as a lumped mass with finite mass moments of inertia, and the shaft's mass is neglected in comparison to the rotor. The *XYZ* reference frame shown in the figure is fixed to a hypothetical undeflected rotating shaft. The frequency of shaft rotation is n, and the total length of the shaft is L.

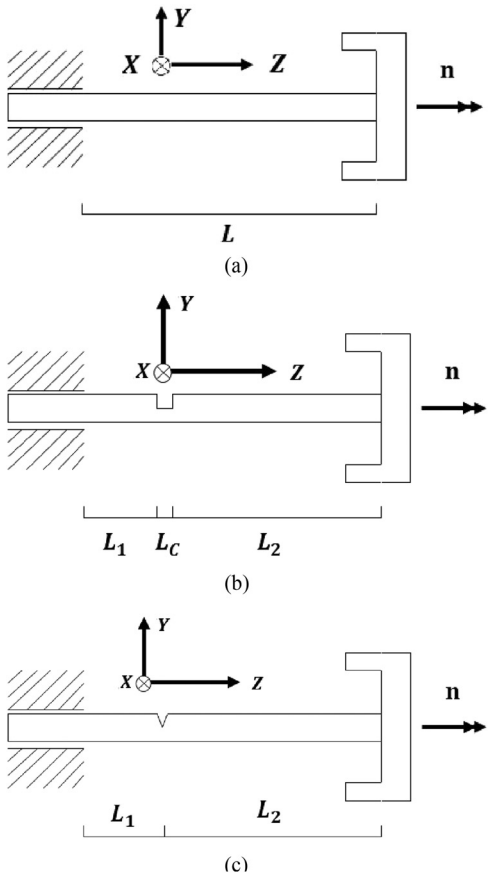

Fig. 1 Comparison of overhung rotordynamic systems: (*a*) undamaged overhung rotordynamic system; (*b*) overhung shaft with notch; (*c*) overhung shaft with gaping fatigue crack

The rotor plane is shown in Fig. 2 to illustrate the degrees of freedom employed. The $x'y'$ axes are shown for clarity in presenting the angular degrees of freedom. Point C designates the rotor's center of mass, which is deflected an amount u_X and u_Y from point O, the undeflected position of C. The reference frame is attached at O and rotates at the shaft speed n. The relationship between the rotating frame XYZ and inertial frame $\xi\eta\zeta$ is shown in Fig. 3. The use of the rotating frame XYZ is advantageous for the analysis, as the stiffness of the shaft is constant relative to the frame. However, the results must be transformed back into the inertial frame, as the condition monitoring system observes the inertial response.

As indicated, the lateral deflection of C is captured by u_X and u_Y in the rotating frame and u_ξ and u_η in the inertial frame.

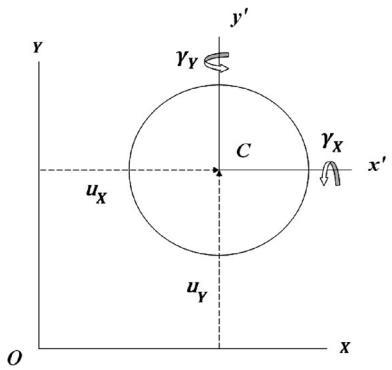

Fig. 2 Rotor degrees of freedom

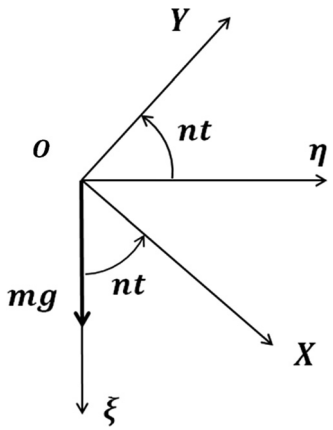

Fig. 3 Relationship between inertial and rotating reference frames

Two orthogonal tilts γ_X and γ_Y provide the rotor's angular motion (γ_ξ and γ_η in the inertial frame). Axial deflection along Z is neglected, along with torsional deformation of the shaft. The vector of rotating frame degrees of freedom $\{q\}$ is

$$\{q\} = \{\, u_X \quad u_Y \quad \gamma_X \quad \gamma_Y \,\}^T \tag{1}$$

A detailed development of the equations of motion is provided by Varney [22]. The general form of the 4×4 linear equations of motion is

$$[M]\{\ddot{q}\} + ([D] + [G])\{\dot{q}\} + ([C]^{-1} - [E])\{q\} = \{F\} \tag{2}$$

where $[M]$ is the mass matrix, $[D]$ is the damping matrix, $[G]$ the gyroscopic matrix, $[C]$ the compliance matrix, and $[E]$ a matrix containing centripetal terms. A general vector of external forces is represented by $\{F\}$. The mass matrix and gyroscopic matrix are, respectively,

$$[M] = \begin{bmatrix} m & 0 & 0 & 0 \\ 0 & m & 0 & 0 \\ 0 & 0 & J_t & 0 \\ 0 & 0 & 0 & J_t \end{bmatrix} \tag{3}$$

and

$$[G] = \begin{bmatrix} 0 & -2mn & 0 & 0 \\ 2mn & 0 & 0 & 0 \\ 0 & 0 & 0 & n(J_p - 2J_t) \\ 0 & 0 & -n(J_p - 2J_t) & 0 \end{bmatrix} \tag{4}$$

while the matrix containing centripetal terms is

$$[E] = \begin{bmatrix} mn^2 & 0 & 0 & 0 \\ 0 & mn^2 & 0 & 0 \\ 0 & 0 & -n^2(J_p - J_t) & 0 \\ 0 & 0 & 0 & -n^2(J_p - J_t) \end{bmatrix} \tag{5}$$

The mass of the rotor is m and the transverse and polar mass moments of inertia are J_t and J_p, respectively. The compliance matrix $[C]$ is the inverse of the stiffness matrix $[K]$. The stiffness matrix of the undamaged overhung shaft with a constant, symmetric cross section is obtained from Euler–Bernoulli beam theory

$$[K] = \begin{bmatrix} \frac{12EI}{L^3} & 0 & 0 & -\frac{6EI}{L^2} \\ 0 & \frac{12EI}{L^3} & \frac{6EI}{L^2} & 0 \\ 0 & \frac{6EI}{L^2} & \frac{4EI}{L} & 0 \\ -\frac{6EI}{L^2} & 0 & 0 & \frac{4EI}{L} \end{bmatrix} \tag{6}$$

where the elastic modulus of the shaft is E and the area moment of inertia of the undamaged shaft is I. The damping in the system is assumed to be proportional to the stiffness of the undamaged shaft by the coefficient β

$$d_{ij} = d_{ji} = \frac{1}{2n}\beta k_{ij} \tag{7}$$

where d_{ij} is a general entry in the damping matrix $[D]$. The coefficient β is experimentally determined by Casey [23] to be approximately 0.01. It is assumed that the crack does not influence the damping; hence, $[D]$ remains proportional to Eqs. (6) by (7) for both crack models.

In a rotating frame, gravity acts as force rotating opposite the direction of the shaft rotation (see Fig. 3). The forcing vector $\{F\}$ containing gravity and imbalance in the rotating frame becomes

$$\{F\} = \begin{Bmatrix} mg\cos(nt) + m_e\varepsilon n^2\cos\theta \\ mg\sin(nt) + m_e\varepsilon n^2\sin\theta \\ 0 \\ 0 \end{Bmatrix} \tag{8}$$

where t is time and g is the acceleration due to gravity. The imbalance of magnitude $m_e\varepsilon$ is shown in Fig. 4 and is oriented as shown. The xy frame shown in the figure is a rotor-fixed frame. Forcing in a constant inertial direction (such as gravity) along with a stiffness asymmetry (such as a gaping crack) is responsible for the appearance of the 2X harmonic [11,14], whereas imbalance is responsible for a 1X harmonic.

The imbalance is only accounted for qualitatively in Eq. (8). In fact, it can be shown that the terms in Eq. (8) constitute a major component of the actual imbalance excitation. The imbalance influences the angular degrees of freedom by coupling the tilt of the rotor to the acceleration of its center of mass. However, as Lee and Green [3] demonstrated, these nonlinear coupling effects are of second order and can, thus, be neglected. Due to linearity, the solution to Eq. (2) is a superposition of the response to imbalance and the response to gravity. As the gaping crack under the influence of gravity solely generates a 2X harmonic in steady state, while imbalance generates only a 1X harmonic, it is hypothesized that the presence of imbalance does not influence the 2X harmonic.

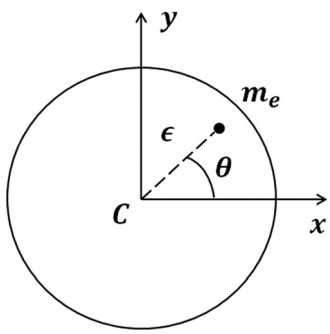

Fig. 4 Rotor imbalance

2.2 Rotordynamic System Displaying Notch. The similarity between manufactured notches and true fatigue cracks allows for a notch to be used as a development tool for establishing crack detection and diagnosis principles. Guidelines can be established experimentally using the notch prior to the complicated manufacture and characterization of a true fatigue crack. As will be seen, the additional compliance introduced by the notch is caused by a reduction in the area moments of inertia of the notched shaft segment.

The cross section of the notched shaft displaying a notch (or crack) of depth a is shown in Fig. 5. When u_X and u_Y are zero, the XY frame shown in the figure reduces to that shown in Fig. 1. The rotating frame always maintains its orientation relative to the notch/crack edge. The uncracked section of the circular shaft of radius R is represented by hatching, and the half-width of the crack is b.

An overhung rotordynamic system displaying a notch of width L_C is shown in Fig. 1(*b*). The distance to the left end of the notch is L_1, while the distance from the notch to the free end of the shaft is L_2. Castigliano's theorem [24] is used in conjunction with Euler–Bernoulli beam theory to derive the global compliance matrix of the notched shaft. The application of a load P_i (about axis i) induces an internal bending moment M_j (about axis j). The applied load can be either a force or moment. In general, the linear deflection u_i caused by the internal bending moment induced by load F_i is

$$u_i = \int_0^L \frac{M_j}{EI_j}\left(\frac{\partial M_j}{\partial F_i}\right)dz \tag{9}$$

while the angular deflection due to applied moment P_i is

$$\gamma_i = \int_0^L \frac{M_i}{EI_i}\left(\frac{\partial M_i}{\partial P_i}\right)dz \tag{10}$$

Note that the area moment of inertia I_j is computed about the axis defined by the direction of the internal bending moment (indicated by the corresponding subscripts). The compliance matrix $[C]$ for a notched shaft is found from application of Castigliano's theorem to be

$$\begin{Bmatrix} u_X \\ u_Y \\ \gamma_X \\ \gamma_Y \end{Bmatrix} = \begin{bmatrix} C_{11_Y} & 0 & 0 & C_{12_Y} \\ 0 & C_{11_X} & -C_{12_X} & 0 \\ 0 & -C_{21_X} & C_{22_X} & 0 \\ C_{21_Y} & 0 & 0 & C_{22_Y} \end{bmatrix} \begin{Bmatrix} F_X \\ F_Y \\ M_X \\ M_Y \end{Bmatrix} \tag{11}$$

where

$$C_{11_j} = \frac{1}{3E}\left(\frac{L_2^3}{I_j} + \frac{(L_2+L_C)^3 - L_2^3}{I_j^C} + \frac{(L_2+L_C+L_1)^3 - (L_2+L_C)^3}{I_j}\right) \tag{12}$$

$$C_{12_j} = C_{21_j} = \frac{1}{2E}\left(\frac{L_2^2}{I_j} + \frac{(L_2+L_C)^2 - L_2^2}{I_j^C} + \frac{(L_2+L_C+L_1)^2 - (L_2+L_C)^2}{I_j}\right) \tag{13}$$

$$C_{22_j} = \frac{1}{E}\left(\frac{L_2}{I_j} + \frac{L_C}{I_j^C} + \frac{L_1}{I_j}\right) \tag{14}$$

The area moment of inertia of the uncracked section is represented by I_j, where the subscript indicates the axis about which the area moment of inertia is computed. The area moment of inertia about axis j of the notched section is represented by I_j^C. The notch area moments of inertia are provided by Varney and Green [2].

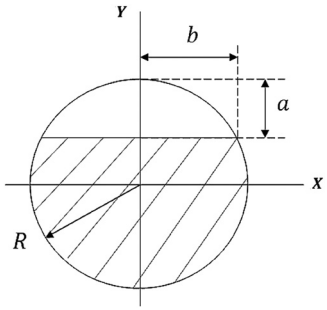

Fig. 5 Cross section of shaft containing transverse crack

The interplay between crack location and depth is evident from Eqs. (11)–(14), as both the notch area moments of inertia and the location of the notch influence the global system stiffness. Details of the derivation are provided by Varney [22]. As expected, the compliance matrix of the notched shaft reduces to that of the undamaged shaft, Eq. (6), when the area moments of inertia are equivalent or the width and/or depth of the notch is set to zero.

2.3 Rotordynamic System Displaying Gaping Fatigue Crack. A gaping fatigue crack (GFC) differs from a notch in that the crack's width is assumed to be negligible. As the name suggests, the mechanism driving the formation of GFCs is fatigue. Fatigue cracks terminate in a sharp edge and are capable of propagation. Therefore, it is hypothesized that a GFC is more likely to be encountered in the operation of real turbomachinery systems than a notch. The cross section of the crack is shown in Fig. 5. A shaft displaying a GFC a distance of L_1 from the cantilevered end is shown in Fig. 1(*c*).

The global compliance of the cracked shaft is a function of the uncracked shaft compliance and the additional compliance introduced by the crack. Dimarogonas et al. [11,12,18] were instrumental in developing a fracture mechanics technique for estimating the local crack compliance using the strain energy release rate and linear elastic fracture mechanics. The concept was extended to rotordynamic systems of six degrees of freedom by Dimarogonas [25]. Here, the dimension of the local crack compliance matrix is reduced from six to four, as axial and torsional deflection are neglected. The crack compliances c_{ij}, which depend on crack depth, relate the shear force V and bending moment M applied to the crack to the displacements u and γ according to [25]

$$\begin{Bmatrix} u_X \\ u_Y \\ \gamma_Y \\ \gamma_X \end{Bmatrix} = \begin{bmatrix} c_{22} & 0 & 0 & 0 \\ 0 & c_{33} & 0 & 0 \\ 0 & 0 & c_{44} & c_{45} \\ 0 & 0 & c_{54} & c_{55} \end{bmatrix} \begin{Bmatrix} V_X \\ V_Y \\ M_Y \\ M_X \end{Bmatrix} \tag{15}$$

The global compliance matrix $[C]$ of the cracked overhung shaft, as seen in Eq. (2), is derived by Varney [22] using the transfer matrix method

$$[C] = \begin{bmatrix} \Delta_{11} & -c_{45}L_2^2 & c_{45}L_2 & \Delta_{14} \\ -c_{45}L_2^2 & \Delta_{22} & \Delta_{23} & -c_{45}L_2 \\ c_{45}L_2 & \Delta_{32} & \Delta_{33} & c_{45} \\ \Delta_{41} & -c_{45}L_2 & c_{45} & \Delta_{44} \end{bmatrix} \tag{16}$$

The terms in the compliance matrix are

$$\Delta_{11} = c_{22} + c_{44}L_2^2 + \frac{(L_1+L_2)^3}{3EI} \tag{17}$$

$$\Delta_{22} = c_{33} + c_{55}L_2^2 + \frac{(L_1+L_2)^3}{3EI} \tag{18}$$

$$\Delta_{33} = c_{55} + \frac{(L_1+L_2)}{EI} \tag{19}$$

$$\Delta_{44} = c_{44} + \frac{(L_1+L_2)}{EI} \tag{20}$$

and

$$\Delta_{14} = \Delta_{41} = c_{44}L_2 + \frac{(L_1+L_2)^2}{2EI} \tag{21}$$

$$\Delta_{23} = \Delta_{32} = -c_{55}L_2 - \frac{(L_1+L_2)^2}{2EI} \tag{22}$$

where I is the area moment of inertia of the uncracked shaft cross section. Once again, note that both the location and depth of the crack substantially influence the global compliance. When the local crack compliances are negated, the compliance matrix reduces to that of an Euler–Bernoulli beam of length $L_1 + L_2$, as expected.

3 Analysis

The equations of motion for both crack models must be solved for a range of crack depths and locations, over a range of viable shaft speeds. The forced equations of motion (Eq. (2)) are placed in a state-space form and solved numerically using a fourth order Runge–Kutta routine. The time step is selected such that adequate resolution is retained in the steady-state response of the system (determined via the shaft speed, as the steady-state response consists of 1X and 2X harmonics). Small initial conditions are applied, and the steady-state response is extracted following decay of the transient response.

3.1 Transformation Into an Inertial Frame. Following solution of the equations of motion, a vector of rotating frame displacements is available at each time step in the solution. However, condition monitoring systems typically rely on inertial frame measurements. With reference to Fig. 3, the rotating frame degrees of freedom are moved into the inertial frame via the following transformation:

$$\begin{Bmatrix} u_\xi \\ u_\eta \\ \gamma_\xi \\ \gamma_\eta \end{Bmatrix} = \begin{bmatrix} \cos nt & -\sin nt & 0 & 0 \\ \sin nt & \cos nt & 0 & 0 \\ 0 & 0 & \cos nt & -\sin nt \\ 0 & 0 & \sin nt & \cos nt \end{bmatrix} \begin{Bmatrix} u_X \\ u_Y \\ \gamma_X \\ \gamma_Y \end{Bmatrix} \tag{23}$$

where u_ξ and u_η are inertial lateral displacements of the rotor center of mass and γ_ξ and γ_η are inertial angular displacements. It is appropriate here to note that the 2X harmonic actually appears as a 1X harmonic as seen in the rotating reference frame, as the forcing in the rotating frame occurs at frequency n. Transformation of the response into the inertial frame results in the appearance of the 2X harmonic. Further details on this concept are provided by Varney [22].

4 Results

The results presented herein are based on the following parameters, obtained from the test rig discussed by Varney and Green [2]. The 10.2 mm diameter shaft of length 88.9 mm is composed of AISI 4140 steel. The elastic modulus of the shaft is 207 GPa, with a Poisson's ratio of 0.33. The width of the experimentally manufactured notch is approximately 1.0 mm. The 0.57 kg rotor is composed of 440C stainless steel, with polar and transverse mass moments of inertia of 3.85×10^{-4} kg m^2, and 2.37×10^{-4} kg m^2, respectively. The rotor's center of mass is offset axially from the end of the shaft by 10.4 mm.

For each crack model, free and forced response results are presented as follows. First, the response is obtained for a system displaying a fixed-location crack, where only the depth is permitted to vary. These results are presented to compare with previously obtained analytic [1,2] and experimental [2,23] results. In this case, the crack is located 6.35 mm from the support. Next, variations in crack depth and location are investigated, from which conclusions pertaining to diagnostics can be drawn.

4.1 Free Response Analysis. A free response analysis is used to extract the 2X resonance shaft speed, which occurs at half of the first natural frequency [1]. The rotating frame eigenvalues p_r are found from the equations of motion and transformed to the inertial frame using Eq. (24), as discussed by Varney and Green [26]

$$p = p_r + n \tag{24}$$

where p represents the inertial eigenvalue (that is, natural frequency). The damping matrix $[D]$ is omitted for the free response analysis.

4.1.1 Fixed-Location Results. Concerning the fixed-location crack, Fig. 6 provides the 2X resonance shaft speed for both crack models versus crack depth. As expected due to the experimental manufacture of a notch, the results in the figure indicate that the experimental results align closer to the notch than the GFC. It is also evident that the two models provide virtually identical results until approximately 20% depth. The models remain similar from 20% to 40% crack depth, though the 2X resonance shaft speed for the GFC begins to decrease more pronouncedly. Beyond 40% depth, the models diverge significantly.

The experimental results fall between those predicted by the two crack models, though slightly less than the predicted notch results. The deviation indicates that the experimental notch contains an additional compliance not captured by the notch model. It is hypothesized that the additional compliance arises due to stress concentrations at the base of the notch.

Figure 6 exposes several qualitative observations concerning crack detection. First, and most importantly, the detection of small cracks using the 2X resonance shaft speed is very difficult for relatively small cracks ($< 20\%$). Second, as the crack becomes more severe, and thus more likely to fail catastrophically, the crack becomes substantially easier to detect (as evidenced by the precipitous decline in the 2X resonance shaft speed beyond 40% depth).

4.1.2 Variable Crack Location Results. Following extraction of the eigenvalues from the equations of motion, Figs. 7(*a*) and 7(*b*) provide contours of the 2X resonance shaft speed for each crack model over a range of viable crack depths and locations (the term "percent location" refers to L_1 expressed as a percentage of the total shaft length). Several important observations can be

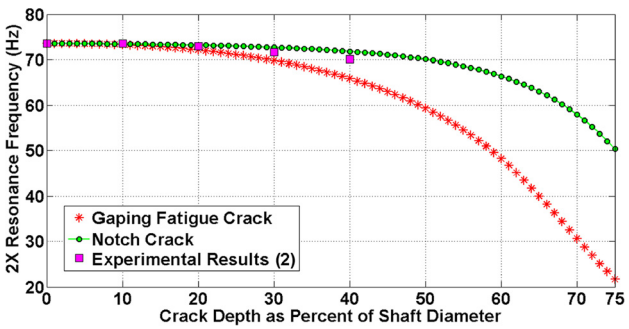

Fig. 6 2X resonance shaft speed versus crack depth for a fixed-location crack

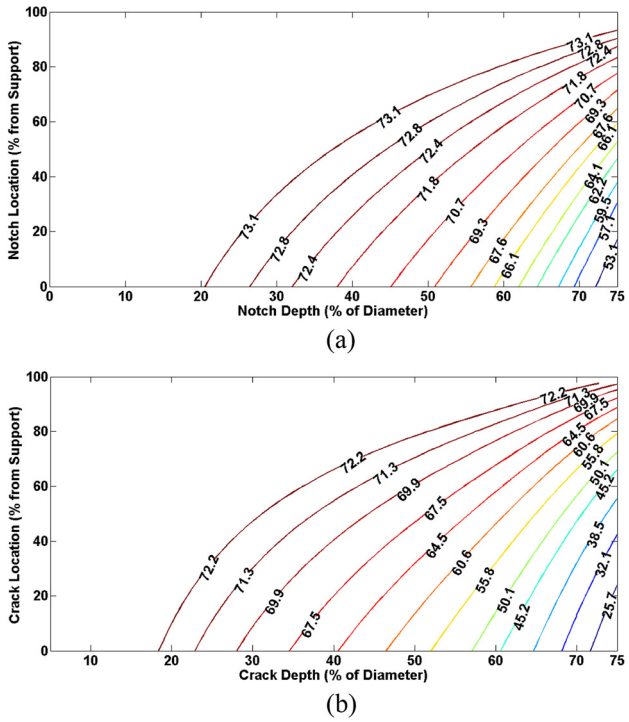

Fig. 7 Free response contour plot: 2X resonance shaft speeds: (*a*) notch; (*b*) gaping fatigue crack

gleaned from these figures. First, measurement of the 2X resonance shaft speed alone is insufficient for diagnosing both the crack location and depth. Knowledge of the 2X resonance shaft speed merely places the possible crack depth and location on a single contour. Second, the difficulty in detecting small cracks or cracks far from the support is clear by the lack of contour differentiation in the leftmost region of the plot (not displayed due to plot resolution). Hence, to detect cracks in the leftmost region, the 2X resonance shaft speed must be measured with a high degree of accuracy.

Last, and perhaps most interestingly, each 2X resonance shaft speed contour begins at a specific crack depth and likewise terminates at a specific crack location. This observation has important implications for qualitatively assessing the severity of a crack, given only the 2X resonance frequency, as a minimum crack depth and maximum crack location can be obtained from a single measurement. Recognition of this possible range of crack depth and location provides the operator with an immediate sense of crack severity and a reduced search region for further search and detection.

4.2 Forced Response Analysis. The magnitude of the rotor's angular response provides a second vibration signature for distinguishing crack depth from location. The angular response of the rotor is used here due to the unique nature of the overhung test rig and monitoring system. Different rotordynamic systems, such as a Jeffcott rotor, would perhaps require analysis using the lateral rotor displacements. Once again, a fixed-location crack is first studied for comparison to previous results [1,2]. Next, the forced equations of motion are solved for many crack depths and locations, thus providing the vector sum of the rotor tilts γ_ξ and γ_η.

4.2.1 Fixed-Location Results. The forced equations of motion, Eq. (2), are solved for a single crack depth-location pair ($a = 40\%$, $L_1 = 6.35$ mm). The rotating frame results are subsequently moved into the inertial frame $\xi\eta\zeta$ using Eq. (23). The steady-state response is extracted from the total response and transformed into the frequency domain using a fast Fourier transform (FFT).

Figure 8(*a*) provides the steady-state response of γ_ξ for a shaft speed of 100 Hz, including both gravity and imbalance. Though the results are presented for a GFC ($a = 40\%$, $L_1 = 6.35$ mm), similar results for the notch are given by Varney [22]. Two components are present in the steady-state response: a 1X harmonic due to imbalance and a 2X harmonic caused by the crack in the presence of gravity. Due to linearity, imbalance does not influence the magnitude of the 2X harmonic, and the crack does not influence the 1X harmonic. Therefore, in the analyses that follow, imbalance is omitted for clarity in presenting the 2X harmonic.

Similar results for a range of shaft speeds are given in Fig. 8(*b*). It is evident from the figure that shaft speeds far from resonance result in a small 2X harmonic (highlighted in the figure). Near resonance, the magnitude of the 2X harmonic increases dramatically. Hence, cracks are difficult to detect using the 2X harmonic when the shaft speed is far from resonance. As will be seen, the magnitude of the 2X angular resonance can be used along with the 2X resonance shaft speed to assist in distinguishing crack depth from location.

4.2.2 Variable Crack Location Results. Figure 9 gives magnitude contours of the 2X angular resonance for a range of shaft speeds and crack depth/location pairs for the GFC. As the crack becomes shallower and further from the support, the magnitude of the resonance decreases significantly; crack detection and diagnosis in this regime can, therefore, be difficult. Similar results are obtained for the notch and are omitted here for brevity (see Varney [22] for the notch results). Double-valued 2X resonance magnitudes are observed in the GFC results for some crack depths. These phenomena are attributed to the changing relationship between the coupling coefficient c_{45} and the other compliance coefficients.

The magnitude of the 2X angular resonance is then extracted for the crack depth and location pairs constituting a single 2X resonance shaft speed contour (see Fig. 7). Pairs of crack locations and depths are obtained by assigning a range of desired crack depths (i.e., 10% to 60%) and iterating the crack location until the target 2X resonance shaft speed is obtained. The results of such a procedure for the GFC are provided in Figs. 10(*a*) and 10(*b*), for

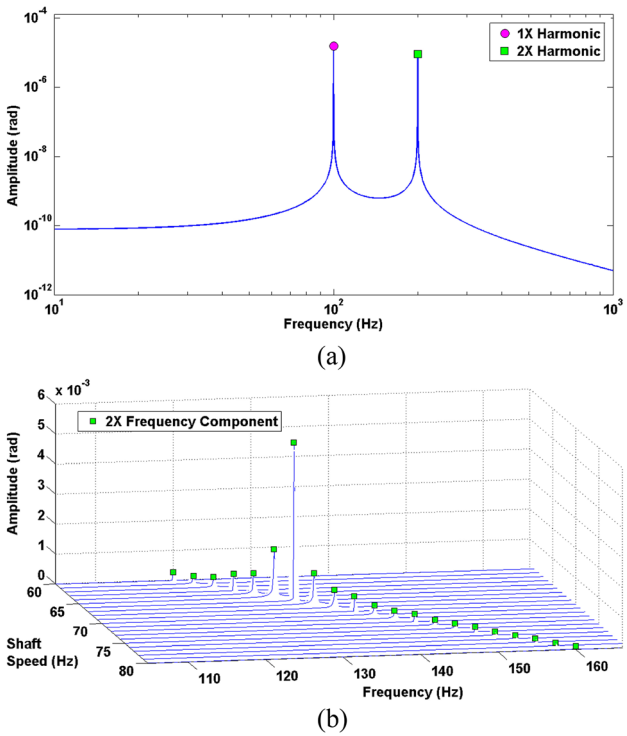

Fig. 8 Forced response of a gaping fatigue crack: (*a*) forced response including imbalance and gravity, at $n = 100$ Hz; (*b*) forced response over a range of shaft speeds to demonstrate the 2X resonance shaft speed

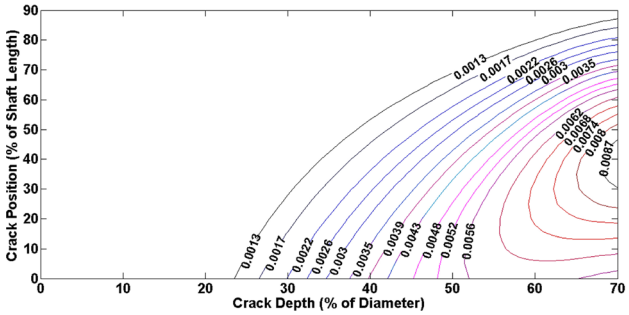

Fig. 9 Magnitude contours of 2X angular resonance (in radians) versus crack location and depth

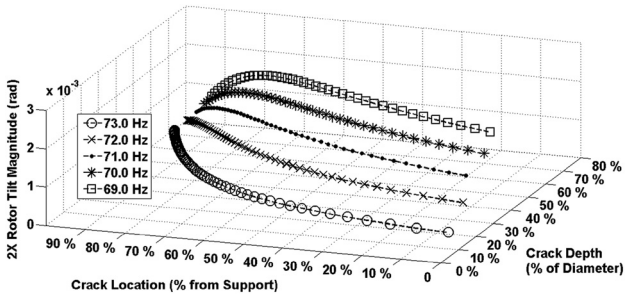

Fig. 11 Loci of 2X angular resonance magnitude for many 2X resonance shaft speeds

2X resonance shaft speed contours of 73 Hz and 70 Hz, respectively. The term "pair number" refers to the crack percent depth composing the pair; hence, a pair number of "40" refers to a crack depth of 40% and the corresponding crack position required to generate the desired 2X resonance shaft speed. Figure 11 gives many such loci versus crack depth and location.

5 Proposed Diagnostic Procedure

A proposed procedure for crack parameter diagnostics based on the prior analytical results is summarized as follows:

(1) Vary the shaft speed of the system and record the 2X resonance shaft speed.
(2) Identify the measured 2X resonance shaft speed contour (giving a range of possible crack depths/locations).
(3) Measure the magnitude of the 2X angular resonance.
(4) Compare the 2X resonance magnitude to a known locus of magnitudes for the specific 2X resonance shaft speed contour (see Fig. 11).
(5) Identify the specific crack depth and location, or provide a reasonable range of estimates.

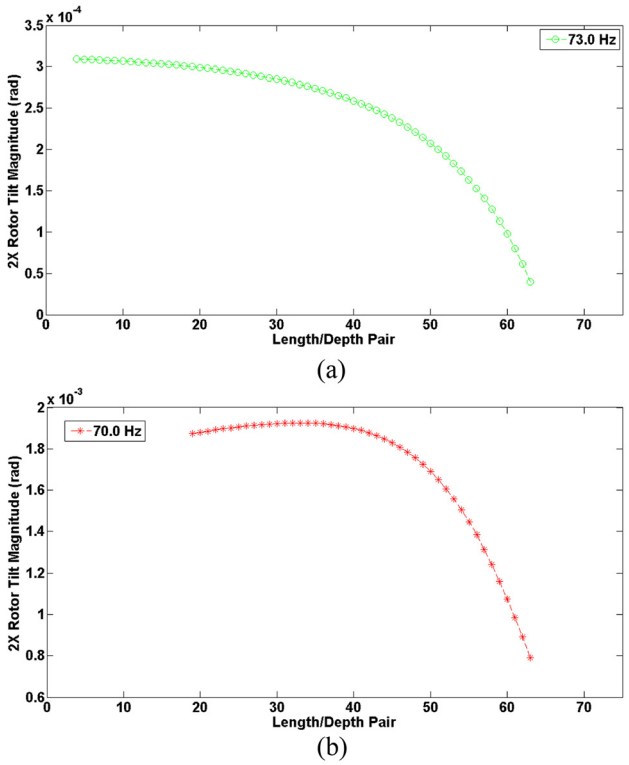

Fig. 10 Locus of 2X angular resonance magnitudes for a range of crack depth and location pairs: (*a*) 73 Hz 2X resonant contour; (*b*) 70 Hz 2X resonant contour

Figure 10(*b*) indicates that some crack depth and location pairs generate the same parameters (2X resonance shaft speed and 2X angular resonance magnitude). If two possible pairs exist, it is likely that either (a) the pair containing the shallower crack is the culprit, considering the time required to propagate the crack or that (b) the crack has formed at the location with the higher stress concentration and stress magnitude. It is concluded that the profile of the 2X angular response is capable of diagnosing crack location and depth.

5.1 Practical Limitations and Shortcomings. To experimentally realize the aforementioned procedure, accurate measurements of the 2X resonance shaft speed and resonant magnitude are crucial, especially to detect shallow cracks or cracks close to the rotor (qualitatively evident by the large regions displaying little change in Fig. 7). Furthermore, observing Fig. 10, angular responses as small as $0.5(10)^{-4}$ rad must be measured to distinguish crack location and depth. Most importantly, the system model must emulate the actual system to realistically distinguish crack depth and location. The model must accurately account for damping, support conditions, and other system parameters to obtain a reasonable estimate of the 2X resonance shaft speed and resonance magnitude.

The results in this work also illustrate the difficulty of transverse fatigue crack detection and diagnosis. It is clear from Fig. 8(*b*) that the 2X harmonic is small when the shaft speed is far from resonance. Severe cracks can exist without detection if the shaft speed is far from resonance or if the crack is located near the overhung rotor.

Crack diagnostics is intimately dependent on the specific system under investigation. The results and conclusions given here are valid specifically for the overhung rotordynamic system discussed, as the angular degrees of freedom are measured in the test rig. However, the signatures of interest (2X resonance shaft speed and the magnitude of the 2X resonance) could also be found using the lateral degrees of freedom of a Jeffcott rotor, for example. The principles discussed herein are, thus, broadly applicable. Related to the nature of the specific system is the placement of the condition monitoring transducers. In this case, the rotor's angular deflection is employed for diagnostics (and, hence, in the test rig discussed by Varney and Green [2], the probes provide the rotor's tilt). Probes are typically placed on the bearings, where the shaft deflection is often minuscule (leading to a poor vibration signal). The probes should, therefore, be placed such that they extract the largest possible response.

Also of concern is that other rotordynamic faults are known to result in a 2X harmonic response, such as misalignment [27] and rotor/stator rubbing contact [3,28]. In the case of a multiple fault situation, additional analysis is required to distinguish the faults. For example, rotor/stator rubbing results in strong backward

whirling character of the 2X harmonic, whereas a crack results in a 2X harmonic that is almost entirely forward whirling [28]; full spectrum analysis is capable of distinguishing these faults. Misalignment, however, results in 1X, 2X, and 3X harmonics [27], whereas a gaping crack only generates a 2X harmonic. Though a gaping crack does not uniquely generate a 2X harmonic, additional analysis techniques and vibration signatures are available to assist in distinguishing multiple faults.

The focus of this work is the diagnosis of gaping fatigue crack parameters using the profile of the 2X harmonic near the 1/2 critical speed (i.e., 2X resonant shaft speed). Breathing cracks, however, generate multiple harmonics, such as a 1X, 2X, 3X, etc. The principles established in this work are equally applicable to these additional harmonics, as each creates a unique subharmonic resonance profile. Therefore, the conclusions of this work are valuable whether the crack is considered open or breathing; in fact, the additional subharmonic resonances induced by a breathing crack may actually aid in the diagnosis of crack parameters.

6 Conclusion

Equations of motion of an overhung rotordynamic system are developed in a rotating frame, where the degrees of freedom are two displacements of the rotor and two tilts. Two gaping crack models are developed: a finite-width notch and a gaping fatigue crack. The compliance matrix for each is derived, indicating that both the depth and location of the crack play an important role in the determination of the global stiffness. Free and forced analyses are performed, and the results transformed into an inertial reference frame.

The free response analysis indicates that the 2X resonance shaft speed alone is insufficient for fully diagnosing the crack parameters (though measurement of this shaft speed can provide crack detection information or a range of feasible crack severity). The steady-state magnitude of the 2X angular resonance is then used to provide a second parameter for diagnosis. A procedure is suggested by which measurement of these quantities can provide an estimate of the crack's depth and location. Additionally, qualitative aspects of crack detection and diagnosis are discussed, namely, the difficulty in detecting cracks using the 2X harmonic when the crack is either shallow, close to the rotor, or the shaft speed removed from the 2X resonance shaft speed. The procedure indicates that it is indeed possible to employ a simple vibration signature, the 2X harmonic, to detect a transverse fatigue crack and diagnose its parameters.

The primary goal of this work is not to present a foolproof method to distinguish crack location and depth but instead to demonstrate the possibility of employing sensible, simple, and typical condition monitoring signals for crack diagnostics. Many qualitative aspects of the results can be employed by an operator to narrow the possible combinations of crack depth and location when a crack is suspected or to provide a warning sign for a dangerously propagating fatigue crack. In this manner, the dynamic interplay between crack depth and location can be better understood and accounted for in transverse fatigue crack detection and diagnosis.

Acknowledgment

This material is based upon work supported by the National Science Foundation under Grant No. 1100101.

Nomenclature

a = crack depth
b = crack half-width
$[C]$ = compliance matrix
E = elastic modulus
$[E]$ = matrix containing centripetal terms
$\{F\}$ = forcing function vector
$[G]$ = gyroscopic matrix
I = area moment of inertia of uncracked beam
I^C = area moment of inertia of cracked beam
J_p = polar mass moment of inertia
J_t = transverse mass moment of inertia
L_1 = crack location from support
m = rotor mass
$[M]$ = mass matrix
n = shaft speed
u_X, u_Y = deflections in the X and Y directions
β = damping coefficient
γ_X, γ_Y = rotating frame angular deflections

References

[1] Green, I., and Casey, C., 2005, "Crack Detection in a Rotor Dynamic System by Vibration Monitoring—Part I: Analysis," ASME J. Eng. Gas Turb. Power, **127**, pp. 425–436.
[2] Varney, P., and Green, I., 2012, "Crack Detection in a Rotordynamic System by Vibration Monitoring—Part II: Extended Analysis and Experimental Results," ASME J. Eng. Gas Turb. Power, **134**(11), p. 112501.
[3] Lee, A. S., and Green, I., 1994, "Higher Harmonic Oscillations in a Non-Contacting FMR Mechanical Face Seal Test Rig," ASME J. Vib. Acoust., **116**, pp. 161–167.
[4] Gasch, R., 2008, "Dynamic Behavior of the Laval Rotor With a Transverse Crack," Mech. Syst. Signal Process., **22**, pp. 790–804.
[5] Green, I., and Etsion, I., 1986, "A Kinematic Model for Mechanical Seals With Antirotation Locks or Positive Drive Devices," ASME J. Tribol., **108**, pp. 42–45.
[6] Green, I., 2008, "On the Kinematic and Kinetics of Mechanical Seals, Rotors, and Wobbling Body," Mechanism Mach. Theory, **43**, pp. 909–917.
[7] Lee, A. S., and Green, I., 1994, "Rotordynamics of a Mechanical Face Seal Riding on a Flexible Shaft," ASME J. Tribol, **116**, pp. 345–351.
[8] Lee, A. S., and Green, I., 1995, "Physical Modeling and Data Analysis of the Dynamic Response of a Flexibly Mounted Rotor Mechanical Seal," ASME J. Tribol., **117**, pp. 130–135.
[9] Darpe, A., Gupta, K., and Chawla, A., 2004, "Coupled Bending, Longitudinal, and Torsional Vibrations of a Cracked Rotor," J. Sound Vib., **269**(1), pp. 33–60.
[10] Darpe, A. K., Gupta, K., and Chawla, A., 2004, "Transient Response and Breathing Behavior of a Cracked Jeffcott Rotor," J. Sound Vib., **272**, pp. 207–242.
[11] Papadopoulos, C. A., 2008, "The Strain Energy Release Rate Approach for Modeling Cracks in Rotors: A State-of-the-Art Review," Mech. Syst. Signal Process., **22**(4), pp. 763–789.
[12] Dimarogonas, A., and Papadopoulos, C. A., 1983, "Vibration of Cracked Shafts in Bending," J. Sound Vib., **91**(4), pp. 583–593.
[13] Mayes, I. W., and Davies, W. G. R., 1976, "The Vibration Behaviour of a Rotating Shaft System Containing a Transverse Crack," *Vibrations in Rotating Machinery*, IMechE, London, pp. 53–64.
[14] Rao, J. S., 1996, *Rotor Dynamics*, 3rd ed., New Age International, New Delhi.
[15] Silva, J., and Gomez, A., 1990, "Experimental Dynamic Analysis of Cracked Free-Free Beams," Exp. Mech., **30**(1), pp. 20–25.
[16] Grabowski, B., 1980, "The Vibration Behavior of a Turbine Rotor Containing a Transverse Shaft Crack," ASME J. Mech. Design, **102**, pp. 140–146.
[17] Gounaris, G. D., and Papadopoulos, C. A., 2002, "Crack Identification in Rotating Shafts by Coupled Response Measurements," Eng. Fract. Mech., **69**, pp. 339–352.
[18] Papadopoulos, C. A., and Dimarogonas, A. D., 1987, "Coupled Longitudinal and Bending Vibrations of a Rotating Shaft With an Open Crack," J. Sound Vib., **117**(1), pp. 81–93.
[19] Quinn, D., Mani, G., Kasarda, E., Bash, T., Inman, D. J., and Kirk, R. G., 2005, "Damage Detection of a Rotating Cracked Shaft Using an Active Magnetic Bearing as a Force Actuator—Analysis and Experimental Verification," IEEE/ASME Trans. Mechatron., **10**(6), pp. 640–647.
[20] Bucher, I., and Ewins, D. J., 2001, "Modal Analysis and Testing of Rotating Structures," Philos. Transact. Ser. A Math. Phys. Eng. Sci., **359**, pp. 61–96.
[21] Penny, J. E. T., and Friswell, M. I., 2007, "The Dynamics of Cracked Rotors," IMAC-XXV: A Conference & Exposition on Structural Dynamics, Orlando, FL, February 19–22, Society for Experimental Mechanics, Bethel, CT.
[22] Varney, P., 2013, "Transverse Fatigue Crack Diagnosis in a Rotordynamic System Using Vibration Monitoring," Master's thesis, Georgia Institute of Technology, Atlanta, GA.
[23] Casey, C., 2000, "Crack Detection in a Rotordynamic System by Vibration Monitoring," Master's thesis, Georgia Institute of Technology, Atlanta, GA.
[24] Budynas, R. G., and Nisbett, J. K., 2008, *Shigley's Mechanical Engineering Design*, 8th ed., McGraw-Hill, New York.
[25] Dimarogonas, A. D., and Paipetis, S., 1983, *Analytical Methods in Rotor Dynamics*, Applied Science Publishers, London.
[26] Varney, P., and Green, I., 2012, "Rotordynamic Analysis Using the Complex Transfer Matrix," Proceedings of the ASME International Design Engineering and Technical Conferences & Computers and Information in Engineering Conference (IDETC/CIE 2012), Chicago, IL, August 12–15.
[27] Patel, T. H., Zuo, M. J., and Darpe, A. K., 2011, "Vibration Response of Coupled Rotor Systems With Crack and Misalignment," IMechE C: J. Mech. Eng. Sci., **225**, pp. 700–713.
[28] Patel, T. H., and Darpe, A. K., 2008, "Vibration Response of a Cracked Rotor in Presence of Rotor-Stator Rub," J. Sound Vib., **317**(3), pp. 841–865.